IBGM
GIF EVALUATIN - 2017
IRAQI BULLETIN OF GEOLOGY AND MINING
Global Impact Factor
0.936

Iraqi Bulletin of Geology and Mining *Vol.14, No.1, 2018* *p 65 – 90*

LANDSLIDE SUSCEPTIBILITY MAPPING USING REMOTE SENSING AND GIS APPLICATION: A CASE STUDY IN QALA DIZA AND SURROUNDING AREA, KURDISTAN REGION, NE IRAQ

Arsalan A. Othman[1], Azad U. Al-Jaff[1], Diary A. Al-Manmi[2] and Ahmed F. Al-Maamar[3]

Received: 25/ 09/ 2017, Accepted: 07/ 12/ 2017
Key words: Landslide, susceptibility, inventory, DEM, Zagros Fold –Thrust Belt, geomorphic indices

ABSTRACT

During the last decades, expansion of settlements into areas prone to landslides in Iraq has increased the importance of accurate landslide inventory and susceptibility studies. The Landslide inventory map is the spatial distribution of the gravity-induced mass movements. Susceptibility mapping provides information about hazardous locations and thus helps to potentially prevent infrastructure damages due to mass wasting. This study aims to assess the localization and size distribution of potential landslides, in addition to implement selected parameters to predict landslide susceptibility using remote sensing techniques in mountainous environments. The study covers the Qala Diza area, Kurdistan Region (NE Iraq), within the Zagros Fold – Thrust Belt, which includes the High Folded Zone (HFZ), the Imbricate Zone (IZ), the Zagros Suture Zone (ZSZ) and the Shalair (Sanandaj – Sirjan) Terrain.

The available reference inventory includes 353 landslides (representing a cumulated surface of 35.38 Km^2) mapped from twelve Quick Bird scenes using manual delineation. The landslide types involve rock falls, translational slides, slumps and toppling which have occurred in different lithological units. At the beginning, cumulative landslide number-size distributions are analyzed using the inventory map. Then, twelve factors, mainly derived from a Digital Elevation Model (DEM) of Shuttle Radar Topography Mission (SRTM), as well as geological and environmental predicting factors were appraised. Logistic regression approaches are used to determine the landslide susceptibility (LS). The areas under the curve (AUC) of the prediction rate curve (PRC) for the landslide susceptibility shows that the accuracy of the map is about 85%. The results indicate that the Hypsometric Integral (HI), lithology and structure are the more significant factors in the detection of potential occurrence of landslides in the studied area.

[1] Iraq Geological Survey, Sulaymaniyah Office, Sulaimaniyah, Iraq, e-mail: arsalan.aljaf@gmail.com
[2] College of Science, Department of Geology, University of Sulaimaniyah, Sulaimaniyah, Iraq, e-mail: diary.amin@univsul.edu.iq
[3] Remote Sensing Sector, Iraq Geological Survey, P.O. Box 986, Baghdad, Iraq, e-mail: ahmedryaman@gmail.com

تقدير احتمالية الانزلاقات الأرضية باستخدام تقنيات التحسس النائي ونظم المعلومات الجغرافية لقلعة دزه والمناطق المحيطة بها، اقليم كردستان، شمال شرق العراق

أرسلان أحمد عثمان، آزاد عثمان الجاف، دياري علي المنمي و أحمد فائق المعمار

المستخلص

خلال العقود الاخيرة، وبسبب التوسع العمراني في المناطق التي تتعرض الانهيالات في العراق ازدادت اهمية اعداد خرائط لجرد احتمالية حدوث الانزلاقات الارضية. تبين هذه الخرائط التوزيع المكاني للانزلاقات الأرضية المحتملة وتزودنا بمعلومات عن الأماكن الخطرة، وبالتالي تساعد على تجنب الخسائر في البنية التحتية بسبب الانهيارات. تهدف هذه الدراسة لتحديد التوزيع المكاني للانهيارات، بالإضافة الى العوامل الأساسية لتخمين احتمالية الانزلاقات باستخدام تقنيات التحسس النائي في المناطق الجبلية. أجريت هذه الدراسة في منطقة قلعة دزة، في إقليم كردستان، شمال شرق العراق ضمن نطاق زاكروس المطوي – المتصدع والذي يتميز بنطاق الطيات العالية، ونطاق التراكب ونطاق الدرز لزاكروس.

تحتوي المنطقة على 353 انزلاق أرضي (تغطي مساحة 35.38 كم^2) تم تحديدها يدويا باستخدام إثنا عشر مرئية كويك بيرد. تشمل الانزلاقات الأنواع التالية: (rock falls, translational slides, slumps and toppling) والتي حدثت في مختلف الوحدات–الصخارية. تم أولا عمل العلاقة التراكمية بين العدد والمساحة للانزلاقات الأرضية ومن ثم تتقييم إثنا عشر عاملا، أغلبها استنبطت من نموذج الارتفاع الرقمي، بالإضافة الى المعاملات الجيولوجية والبيئية. تم استخدام طريقة الـ logistic regression لتحديد خريطة احتمالية الانزلاقات. إن نسبة الدقة المتمثلة بالمساحة تحت منحنى الاحتمالية للانزلاقات كانت حوالي 85%. بينت النتائج ان المعامل الهبسومتري والتنوع الصخاري والبنيوي هي من أكثر العوامل المؤثرة التي تساعد في تحديد الانزلاقات المحتمل حدوثها في منطقة الدراسه.

INTRODUCTION

Several Types of mass movements are included in the common term "landslide", the more restrictive use of the landslide refers only to mass movements (USGS, 2004). Landslides represent a major risk to human life; as well as to private and public properties (Petley, 2012). Landslides include a wide range of ground movements, such as rock falls, deep slope failures and shallow debris, flows. The mass movements can happen in offshore, coastal and onshore environments. Although the action of gravity is the primary driving force for a landslide to occur, there are other contributing factors affecting the original slope stability (Werner and Friedman, 2010). Maps of landslides are classified into three classes: inventory maps, density maps, and susceptibility maps (Guzzetti *et al.*, 2000). Landslide investigations can be categorized into three main groups: **1)** landslide recognition, classification, and post-event analysis, **2)** landslide monitoring, and **3)** landslide susceptibility and hazard assessment (Metternicht *et al.*, 2005).

Guzzetti *et al.* (1999) considered that any mass movement is part of a landslide inventory map. Landslide inventory maps involve landslide detection, recognition and classification. The size is one of the most important aspects in the recognition of landslides (Mantovani *et al.*, 1996). The estimation of the size and probability of landslide occurrence is thus part of any landslide hazard assessment (Fukuoka *et al.*, 2005). Until recently, visual interpretation over aerial photographs and orbital high spatial resolution images remained the major source for landslide inventory map preparation. So far, visual interpretation of landslides with field checking is more accurate than automatic extraction; in many cases. Nonetheless, the accuracy of automatic procedures has increased steadily and thus they are more and more adequate to be used to generate landslide inventory maps.

The landslide susceptibility is defined as a probability of the spatial terrain to trigger a landslide over a set of geoenvironmental conditions (Ozdemir and Altural, 2013). The prediction techniques are based on the popular assumption that “the past and the present landslide locations are the keys to the future" (Capitani *et al.*, 2013, Carrara *et al.*, 1995 and

Van Den Eeckhaut *et al.*, 2006). In other words, slope failures are determined by a given set of controlling factors, and future slope failures are expected to occur under the same conditions (Lee and Talib, 2005). So far, lithology, slope gradient, slope aspect, and distance to streams and lineaments (including fractures) are widely accepted as significant predicting factors for the occurrence of landslides (Capitani *et al.*, 2013, Ozdemir and Altural, 2013 and Wang *et al.*, 2013).

The study area is located between 36° 00' – 36° 30' N latitudes; 45° 00' – 45° 30' E longitudes, in the Zagros Mountains, where mass movements threaten many towns and villages. It covers an area around 1365.1861 Km² and encompasses the Sulaimaniyah Governorate (the Kurdistan Region) in the northeast of Iraq (Fig.1). The main cities and towns in the study area are Qala Diza, Bastah and Bankard. Lesser Zab River, Chami Zharzwa, Rubari Garfen, Chami Sharwet and Chami Bastasten are the main streams, which are flow from the northeast and southeast of the study area. A small part of the Dokan Lake is within the study area too. The study area is characterized by different mountainous ranges. The main ranges and mountains are Bardqalsht, Gazohrahzi, Mara Pasta, Kirkuk, and Garda Mand and Qandeel. The main aims of this study are: **1)** mapping the landslide inventory **2)** assess the localization and size distribution of landslides, and **3)** prediction of landslide susceptibility in the Qala Diza area.

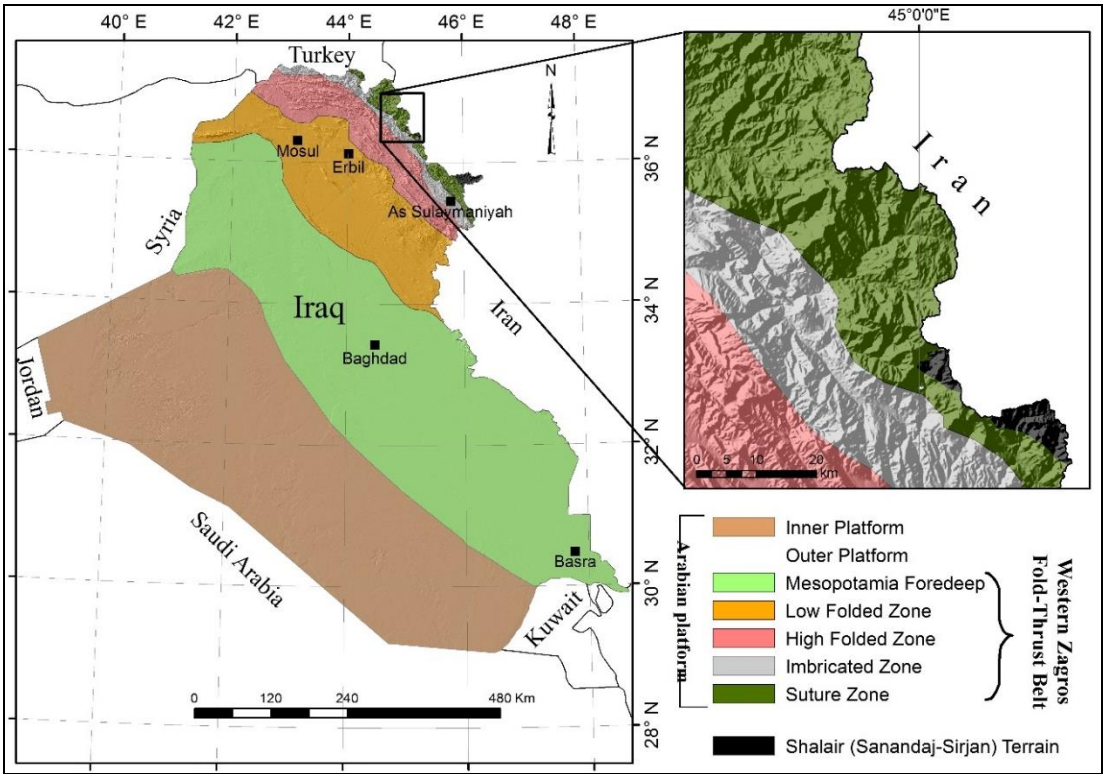

Fig.1: Tectonic map showing the location of the study area, which comprises the High Folded Zone (HFZ), the Imbricate Zone (IZ) and the Zagros Suture Zone (ZSZ) (Fouad, 2012)

CLIMATE

The Qala Diza area is characterized by large seasonal variations in precipitation, temperature, and evaporation, represented by dry summers and wet winters (Fig.2). The

Köppen – Geiger climate classification system (Kottek *et al*., 2006) characterizes the climate as warm temperate with dry and hot summer. Most of the annual precipitation (858.7 mm) occurs from October to May. January shows the highest precipitation with an average value of 198.2 mm. The average monthly temperatures vary between − 0.6 °C (January) and 37.3 °C (August). Snowfalls occur within 10 – 11 days per year on average; between November and April (Fig.2). Above 1.500 m (a.s.l.), heavy snowfall occurs in the winter. Heavy rainfall, heavy snowfall and rapid snow melting subsequent to a sudden change in temperature, lead to the incidence of landslides in the spring.

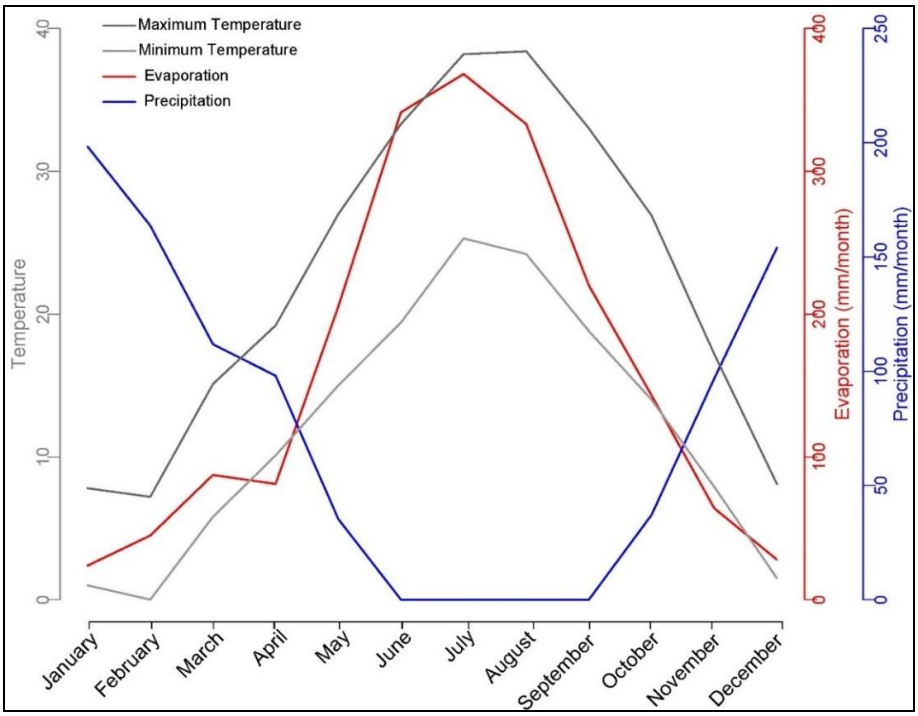

Fig.2: Monthly precipitation, evaporation and maximum and minimum temperatures, in the study area; based on the data from 2000 to 2006 acquired from Qala Diza Meteorological Station

METHODOLOGY

- **Data and Software**

The availability of new satellite sensors with better spatial and spectral resolutions made the use of satellite data more attractive than aerial-photographs to detect and investigate landslides. For this study, 12 cloud-free Quick Bird scenes are used. They were acquired from 18th August 2002 to 29th August 2006. The final product is a 3-bands, 8-bit, 0.6 m resolution mosaic; covering more than 6,554 Km^2. The product has three visible spectral bands in the blue (450 to 520 nm), green (520 to 600 nm) and red (630 to 690 nm), and one panchromatic band (450 to 900 nm). The mosaic does not include the near infrared band (760 to 900 nm). The three visible spectral bands data were pan-sharpened using the University of New Brunswick (UNB) algorithm (Brink *et al.*, 2009). In addition, we have used one scene of 1 Arc-Second Global Shuttle Radar Topography Mission (SRTM) digital elevation mode (DEM) with 30 m resolution. Each scene of SRTM – DEM covers 1 by 1 degree on land. The DEM is used to extract the morphological features. All GIS operations (base map preparation, raster vector conversion, slope, aspect, curvature, distance map, and area calculation) were

performed using ArcGIS10 (ESRI 2011) and all statistical analyses were conducted using R-based scripts.

- **Methods**

Geomorphic indices analysis is a powerful tool to investigate major landslides. The use of geomorphic indices derived from DEM allows the characterization and comparison of landscapes. After subset SRTM DEM, the geomorphic indices such as the HI values and the topographic position index (TPI) were extracted from the SRTM DEM data and analyzed using ArcGIS 10.1.

Inventory Landslides Map is prepared from two sources. First, existing geological maps (Bolton, 1954; Paver and Scholtzh; 1955, Buday and Suk, 1978; Abdulaziz *et al.*, 1983) with mapped landslides, which were scanned and georeferenced. The data is completed, with the visual interpretation and digitization of Quick Bird scenes (partly verified by field survey in different parts of the study area). The landslide boundaries were identified from the satellite data based on many aspects; such as tone, texture, headwall scarps and associations, such as pathway of the material movement and fragments of transferred materials. Varnes (1978) classification is used to classify the landslides. The observations are partly verified by field check in different parts of the study area.

The predictive parameters used in landslide susceptibility analysis for different areas can be arranged according to topographical, geological and environmental factors (Nefeslioglu *et al.*, 2008a). Twelve predictive factors were selected and stored as thematic maps. Some of them, such as TPI and HI, have been seldom used as predictive factors. Thematic maps are resampled in order to have the same spatial resolution as the pixel size of SRTM DEM, (i.e. 30 m spatial resolution). The input factors can be discrete or continuous. Factors such as lithology, land cover and slope aspect are discrete while the other factors, such as elevation and slope gradient, are continuous. The logistic regression model can use both discrete and continuous inputs (Choi *et al.*, 2012).

GEOLOGICAL SETTING

The Zagros Thrust – Fold Belt is part of the Alpine – Himalayan mountain ranges and trends in the NW – SE direction. This belt is around 2000 Km long, extending from SE Turkey through Iraq to southern Iran (Alavi, 1994, Alavi, 2004, Othman and Gloaguen, 2013a, Othman and Gloaguen, 2013b and Othman and Gloaguen, 2015). The study area lies within the High Folded Zone (HFZ), the Imbricate Zone (IZ), the Zagros Suture Zone (ZSZ) and the Shalair (Sanandaj – Sirjan) Terrain (ShT) (Fouad, 2012). The study area is characterized by long and narrow anticlines; some of them exhibit different types of faulting. Twenty five main anticlines with many other minor anticlines of NW – SE direction are identified in the study area (Sissakian, 1998). The geology of Qala Diza area, presented hereinafter, is based on the 1: 100 000 scale map compilations accomplished by Iraq Geological Survey (GEOSURV, 1985).

The Baluti Formation (Late Triassic) is exposed in the HFZ and IZ, whereas, the Sarki and Sehkaniyan formations (Early Jurassic) are exposed in the southern part of the study area, within the HFZ. These three formations cover small area ~16 Km^2; therefore, they are presented together in the geological map. These formations consist of massive dolostones and limestones, very hard, bedded and massive. Naokelekan, Barsarin (Late Jurassic) and Chia Gara formations (Jurassic – Cretaceous) are exposed only in the southern part of the study area. These three formations cover small area ~13.7 Km^2, therefore, they are presented

together in the geological map. They consist of laminated shaley limestone and dolomitic limestone, limestone, thinly bedded bituminous limestone and calcareous shale "coal horizon". Balambo and Sarmord formations (Early Cretaceous) are exposed in the southeastern part of the study area. They trend in the NW – SE direction and cover small area of ~28.3 Km^2; therefore they are presented together in the geological map.

The Balambo Formation consists of thinly bedded limestones with intercalations of green marl and blue shales. The Sarmord Formation consists of limestones and marl with alternations of blue marls and marly limestone. The Qamchuqa Formation (Early Cretaceous) is widely exposed in the study area and consists of dark grey limestone and dolomite. The thickness of the formation is highly variable, ranging from (200 – 1000) m. The Kometan Formation (Late Cretaceous) is exposed in the southeastern part of the study area. It consists of thinly well bedded marly limestone and marl. The Shiranish Formation (Late Cretaceous) is widely exposed in the study area and consists of thinly well bedded white, yellowish white and greyish white marly and chalky limestone, followed (upwards) by thin bedded or papery blue and grey marl, with some marly limestone beds. The thickness of the formation is highly variable ranging from (100 – 500) m. The Tanjero Formation (Late Cretaceous) consists of alternation of dark green and yellowish green shale, claystone, sandstone and siltstone. Some conglomerates occur in the upper part and some marly limestone in the lower part. The thickness of the formation is variable ranging from (200 – 2000) m.

The Gercus Formation (Early – Middle Eocene) consists of red claystone alternated with red siltstone. Sandstones and conglomerate beds may rarely occur in the lower and/ or upper most parts of the formation. The thickness of the formation is variable, in Shaqlawa Koisanjaq area it is 220 m, but decreases in the southeast and northwest directions. The Pila Spi Formation (Middle – Late Eocene) consists of limestone and dolomite, well bedded, hard to very hard, light grey and white in color, with very rare marl and marly limestone. The thickness of the formation is highly variable, ranging from (52 – 120 m). The Fatha Formation (Middle Miocene) consists of reddish brown claystone and marl with alternation of limestone. Reddish brown siltstone and sandstone are also common, especially in the upper cycles. Gypsum is present as minor component in some cycles of the lower part only. The thickness of the formation is variable, ranging from (130 – 310 m). The Injana Formation (Late Miocene) consists of reddish brown sandstone, siltstone and claystone in cyclic nature. The thickness of the formation is variable, ranging from (120 – 2000 m). The Mukdadiya Formation (Late Miocene – Pliocene) consists of grey, coarse grained, friable sandstones with some cyclic beds of pebbly, yellowish grey, claystone and siltstone. The thickness of the formation is highly variable, ranging from 65 – 1000 m (Sissakian, 1998).

The ZSZ is formed by the collision of the Arabian and the Eurasian margins, and the closure of the Neo-Tethys (McQuarrie *et al.*, 2003; Moghadam *et al.*, 2013). The shortening of the Zagros Thrust – Fold Belt resulted from the ongoing subduction of the Arabian Plate beneath the Eurasian Plate during the Late Cretaceous and Miocene – Pliocene (Sissakian, 1998; Jassim and Buday; in: Jassim and Goff, 2006). The ZSZ includes **(1)** Qandil Metamorphosed Series (Cretaceous), exposed north of Qala Diza town along the frontier with Iran, forming the bulk of Qandeel Range. It consists of sheared limestone, phyllite and massive metamorphosed limestone, with some serpentine intrusions. The thickness of this unit is about 3000 m. **2)** Walash Group (Paleocene – Eocene), consists of very thick basic volcanic sequence including agglomerate, lava flows, pillow lavas and ashes with associated dykes. The thickness of the group in the type locality is 1000 m, but in nearby areas is about 3500 m. **3)** Naopurdan Group (Paleocene – Oligocene), consists of grey shale, coralline

limestone, tuffaceous slates, felsitic volcanics, basic conglomerate, greywacke and sandy shale. The thickness of the group, in the type locality is about 2000 m, but this thickness is reduced in the study area to about 1000 – 1500 m, mainly due to thrusting. **4)** Red Bed Series (Paleocene – Miocene), consists of conglomerates, red shale, red sandstones, and red mudstones together with grey shale with sandstones and lenticular limestone (Surgala Red and Grey Beds). Grey shale, occasionally marly with intercalations of thin beds of greywacke and impure very lenticular limestone (Razga Grey Beds). The thickness of the Red Bed Series is about 500 m, but near Qalat Dizeh town it is about 1200 m. **5)** Merga Red Beds (Late Miocene – Pliocene), consist of massive, boulder conglomerate, in the upper part, and red, calcareous, silty shale and sandstones in the lower part. The pebbles of the conglomerate are of igneous and metamorphic origin. The thickness of the beds is 500 m in the study area.

Different types of Quaternary sediments are developed in the study area of Pleistocene to Holocene age, among them are: **1)** The River Terraces (Pleistocene) developed mainly on both sides of the Lesser Zab River. Usually, two levels of terraces are presented in the study area, although many other levels could be present. They are composed of silica and limestone pebbles with some metamorphic and igneous rocks. The size of the pebbles ranges from less than 1 cm up to 20 cm. **2)** The Alluvial Fan Sediments (Pleistocene – Holocene) are formed of rock fragments, mainly of limestone and dolostone, cemented by calcareous and rarely of sandy and silty cement. The thickness is variable; ranging from few meters up to 25 m. **3)** The Slope Sediments (Pleistocene – Holocene), consist mainly of limestone and dolostone fragments with some silicate, igneous and metamorphic pebbles, derived from the exposed formations. These sediments are poorly to moderately cemented by calcareous, sandy and silty materials. Locally, they are well cemented and very hard. The thickness of the slope sediments is widely variable; it ranges from less than one meter up to 20 m. **4)** The Flood Plain Sediments (Holocene), developed mainly along the Lesser Zab River and the large valleys. These sediments consist mainly of sand, silt and clay with rare lenses of gravel. The thickness varies from less than one meter up to 3 m (Fig.3).

LANDSLIDES

Landslides are frequent in the study area and they are triggered by both natural (e.g., slope processes) and anthropogenic (e.g., road cuts or vibrations due to heavy daily traffic) processes (Michoud *et al.*, 2012). In the study area, the main natural factors which may induce landslides are: normal precipitation, focused precipitation, water released after rapid snowmelt in spring, and the relatively heterogeneous geology and geomorphology. Human-induced causes of slope failures include the construction of civil engineering activities, like overloading of the slopes or undercutting of the toe of slopes and unsuitable agricultural practices (Othman and Gloaguen, 2013b).

The most widely used classification scheme developed by Varnes (1978) divides landslides into different types according to the material and the type of movement (Dikau *et al.*, 1996 and Varnes, 1978). This classification distinguishes five types of mass movement (falls, topples, slides, spreads, and flows) in addition to combinations of these principal types along with types of material (bedrock, coarse soils and predominant fine soils).

- **Landslide Inventory Map**

The available reference inventory includes 353 landslides representing a cumulated surface of 35.38 Km^2. Several types of landslides are common in the study area including rock falls and toppling, which occurred independent or collective in different lithological

units along steep slopes and gorges and covere 4.3% of the total landslides in the study area (Table 1). Landslides have caused road blockings and consequently many nearby towns occasionally suffer from such incidents. A large mass of rock fall was witnessed recently in the study area that blocked many main roads. Big blocks of heavily fractured limestone may fall from a steep-slope cliff due to gravity. Rockslide is common in hard rock and occurs along a shear surface, which is planar (Blasio, 2011). This type of slide, in addition to earth slide, covers ~51% of the total landslides of the study area (Table 1). It causes more damage than rock fall and is thus more dangerous. Slumps or spoon-like landslides cover 35.3% of the total landslides of the study area (Table 1), occurring in different lithological units along gentle and steep slopes, gorges, and shear surfaces (Fig.4b). Slump landslides are common in weak layers (rock slump and earth slump), especially when they are softened by percolation of rainwater (Blasio, 2011).

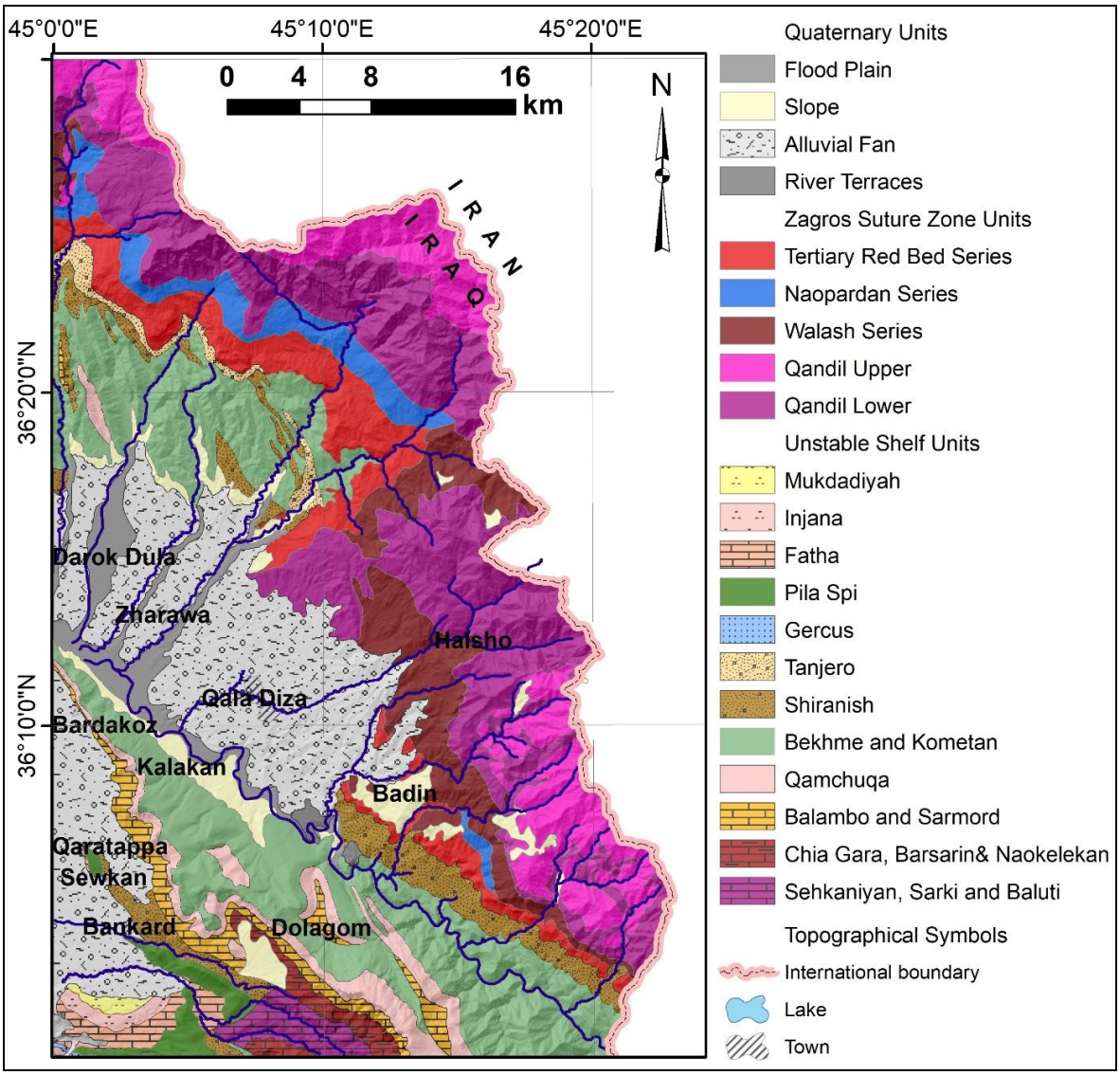

Fig.3: Geological map overlaying the hillshade obtained from SRTM DEM of the Qala Diza area (Sissakian, 1998; Sissakian and Fouad, 2014)

Table 1: Statistical characteristics of the identified landslides in the studied area

Landslides Type	No. of Landslides	Min. Area (m^2)	Max. Area (m^2)	Total Landslides Area (m^2)	Landslides Rate of Total Area %
Earth slump	125	8.99	695,342.84	3,995, 252.46	11.29
Earth flow	73	108.55	927,555.5	3,216,655.05	9.09
Earth slide	8	5,486.62	108,680.25	198,098.5	0.56
Rock fall and toppling	43	59.97	608,621.2	1,530,820.86	4.33
Rock flow	6	3,394.91	59,611.26	119,614.7	0.34
Rock slide	52	138.23	2,654,951.78	17,819,562.54	50.36
Rock slump	46	208.78	1,418,740.96	8,501,239.62	24.03
All types	353	8.99	2,654,951.78	35,381,243.73	100

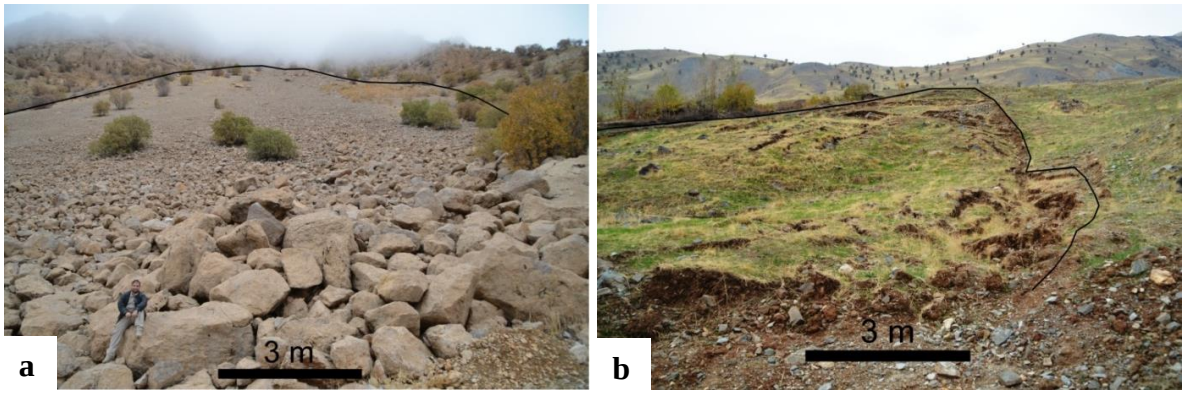

Fig.4: Typical examples of the landslides within the study area
a) rock flow, **b)** earth slump

Figure (5) shows that slump sliding threatens the roads in different sites in the study area. The old and active slump landslides, particularly the large ones, might develop in the future into smaller landslides creating a hazardous effect on engineering structures. Some of the landslides are as old as Early Pleistocene Period (Buday and Suk, 1978). Among the numerous landslides observed in the region, the best examples are those that occurred around the towns of Hero and Halsho (Fig.5c). This area is affected by extensive blocks and slump sliding, which mainly occur on the slopes of deeply eroded valleys and in areas where clay layers underlie hard rocks. In addition, clastic debris and rock flow is common in the weak layers and soil. They cover ~9.4% of the total area of the landslides in the study area (Table 1), especially in the north-northwest parts of the study area where the debris are usually fine-grained.

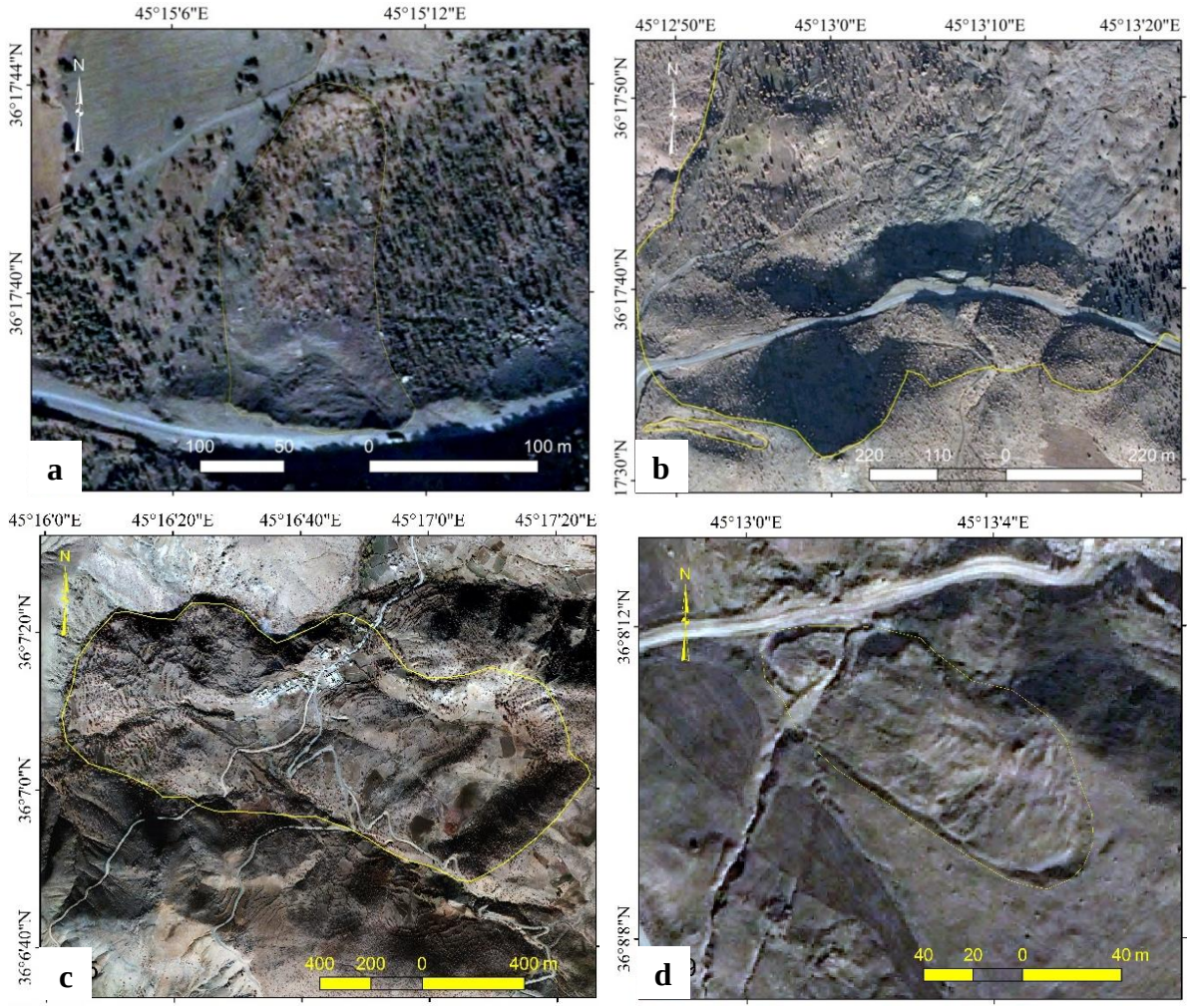

Fig.5: Standard deviation stretch of Quick Bird imagery R3:G2:B1, showing examples of detected landslides in the study area. The four images represent the landslides that were checked in the fieldwork

- **Statistical Characteristics of the Landslides**

A cumulative log landslide number distribution is a graphic plot that shows the relation between log size and log number of landslides (Fujii, 1969). The x-axis represents log size and the y-axis represents log of cumulative number of the landslides. The cumulative distribution allows quantification of the results of the inventory map by determining the statistics of the landslide sizes. The cumulative distribution of the landslides is given by Equation (1):

$$N_{cl} = \beta \times S^{-a} \quad \ldots\ldots\ldots\ldots\ldots\ldots\ldots\ldots\ldots\ldots \quad 1 \text{ (Fujii, 1969)}$$

where: N_{cl} = cumulative number of landslides, α (alpha) = the cumulative exponent, and β (beta) = constant, S = size of landslides. The probability density distribution of 353 landslides within the study area are plotted in Fig. (6b). The bandwidth estimation of kernel density is 0.2566, and reflects large to medium variance in landslide sizes. Figure (6a) shows that there are a limited number of very small and very large landslides in the study area. The maximum distribution of the landslides within the study area ranged from 0.001 to 0.1 Km^2.

In addition, the largest 12 landslides (>1 Km^2) cover a total area of 18.8 Km^2, located in the northeast-east of the study area.

The fit of a power law to the cumulative distribution of event sizes is commonly used to analyze landslide (Brink *et al.*, 2009, Corominas and Moya, 2010, Dai *et al.*, 2011, Guthrie and Evans, 2004, Guzzetti *et al.*, 2002, Pelletier *et al.*, 1997, Sugai *et al.*, 1995 and Van-Den-Eeckhaut *et al.*, 2007). Here, we have calculated the cumulative number-area of the landslides within the Qala Diza area. The cumulative distributions of 353 landslides show statistical correlations > 0.894 (Fig.7). The power exponent is $\alpha = -0.425$.

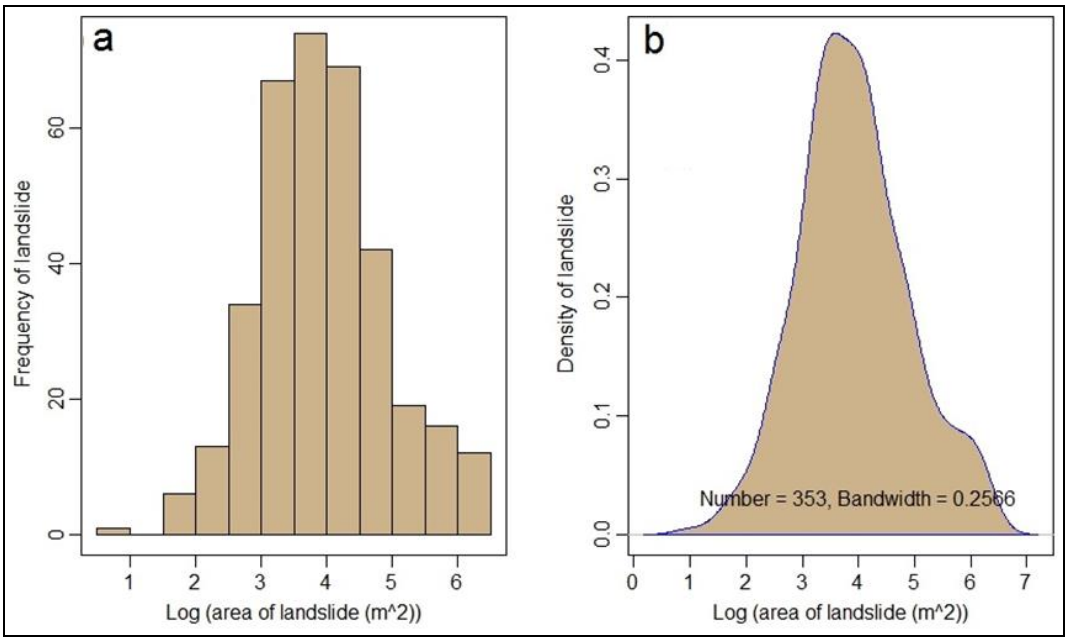

Fig.6: Statistic plots, **a)** Histograms showing the number and size of the landslides in logarithmic coordinates; **b)** Probability density distribution showing 353 landslides within the study area

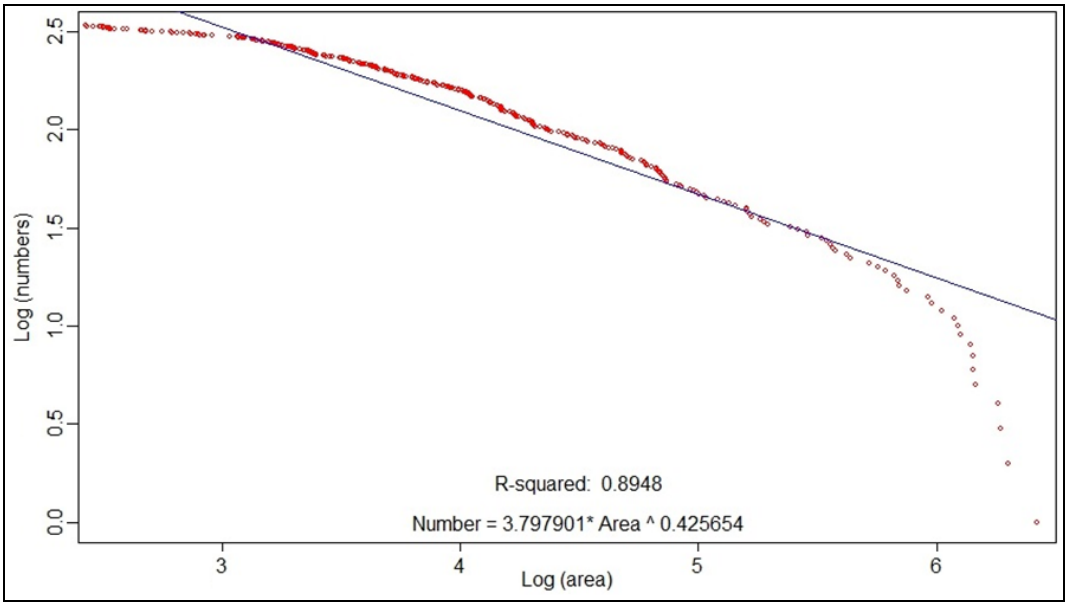

Fig.7: Distribution plot of 353 landslides within the study area

- **Landslide Susceptibility Map**

The landslide inventory map is fundamental for producing the landslide susceptibility map (Zhao *et al.*, 2012). The landslide susceptibility is defined as a probability of the spatial terrain to trigger a landslide over a set of geoenvironmental conditions (Ozdemir and Altural, 2013). Such maps are essential for the estimation of potential regions of landsliding (Guzzetti *et al.*, 2005). In addition, the landslide susceptibility is a fundamental and very useful tool supporting the decision making and planning for land use management (Akgun, 2012). Over the last decades, many different mapping techniques, such as frequency ratio (FR) (Lee and Talib, 2005, Ozdemir and Altural, 2013 and Shahabi *et al.*, 2014), weight of evidence (WoE) (Lee, 2013, Lee *et al.*, 2002 and Ozdemir and Altural, 2013), analytical hierarchy process (Ayalew *et al.*, 2005 and Shahabi *et al.*, 2014), bivariate statistical analyses (Althuwaynee *et al*., 2014 and Ayalew *et al*., 2005), artificial neural networks (Conforti *et al*., 2014, Ercanoglu, 2005, García-Rodríguez and Malpica, 2010, Lee *et al*., 2001 and Qiao *et al*., 2013), support vector machine (Peng *et al*., 2014 and Yao *et al*., 2008) and logistic regression (Atkinson and Massari, 1998, Lee and Min, 2001, Ozdemir and Altural, 2013 and Shahabi *et al.*, 2014) have been implemented for the landslide susceptibility estimation. All these prediction techniques are based on the popular assumption that "the past and the present landslide locations are the key to the future" (Capitani *et al.*, 2013, Carrara *et al.*, 1995, Van Den Eeckhaut *et al.*, 2006 and Zêzere, 1999). According to this assumption, one can also conclude that the authors assumed that slope failures are determined by landslides controlling factors, and the future slope failures will occur under the same conditions as past slope failures (Lee and Talib, 2005).

In addition, the definition of a set of factors that can be used to predict the future occurrences of landslides and to estimate the statistical relationships between the predicting factors for sliding the masses and the occurrences of landslides is the conceptual knowledge of all landslide susceptibility techniques (Capitani *et al*., 2013, Carrara *et al.*, 1995 and Van Den Eeckhaut *et al.*, 2006). The lithology, the slope gradient, the slope aspect, the distance to streams, and to tectonic lineaments are widely accepted as significant factors that are related to the occurrence of landslides (Capitani *et al.*, 2013, Kayastha *et al.*, 2013, Ozdemir and Altural, 2013 and Wang *et al.*, 2013).

- **Input and Preparing Parameters**

Landslide susceptibility maps are produced for the Qala Diza area; where no studies of the landslide susceptibility have been carried out in this area. There is no agreement on which predictive factors have to be used in the landslide susceptibility analyses, but most of the existing works evaluated topographical, geological and environmental factors as essential predictive factors (Nefeslioglu *et al.*, 2008a).

Twelve predictive factors of landslides are prepared, and stored as thematic maps. These factors play a dominant role in the slope stability. These factors are classified into three categories: morphometric, geological, and environmental factors. We reclassified these thematic factor maps to have a similar pixel size of ASTER DEM, i.e. a 15 m spatial resolution. These factors are **(1)** lithology, **2)** land cover, **3)** slope gradient, **4)** slope aspect, **5)** slope curvature, **6)** Hypsometric Integral (HI), **7)** elevation, **8)** distance to drainage, **9)** distance to faults, **10)** distance to roads, **11)** precipitation, and **12)** Topographic Position Index (TPI). GIS techniques are used to produce the landslide susceptibility map using logistic regression model. The input factors can be discrete or continuous. Factors such as lithology, land cover and slope aspect are discrete while the other factors such as elevation

and slope gradient are continuous. The logistic regression model can use both discrete and continuous inputs.

- **Morphometric Factors**

In this study, eight morphometric variables are used which are: **1)** elevation (DEM), which affects the occurrence of landslides and indirectly affects the climatic conditions and hence soil erosion (Ozdemir and Altural, 2013, Wang *et al*., 2013 and Xu *et al*., 2012). The DEM was obtained from SRTM data. The other morphometric parameters were extracted from the DEM (i.e. slope gradient, slope aspect, slope curvature, the HI, elevation, distance to drainage, and TPI). Elevation in the study area ranges from 475 to 3148 m a.s.l. (Fig.8A) with the highest values in the north and northeast of the study area. **2)** Slope gradient, which is the major factor of slope stability analysis. The maximum slope gradient is 77° (Fig.8B). **3)** Slope aspect, which is associated to solar radiation, wind, and rainfall (Lee and Min, 2001 and Yalcin *et al.*, 2011). Slope aspect is assumed to have an impact on vegetation cover and; therefore, may affect the occurrence of landslides (García-Rodríguez *et al*., 2008). Figure (9A) shows the slope aspect distribution in the Qala Diza area. **4)** Slope curvature (Nefeslioglu *et al*., 2008b), ranges from positive to negative. A positive value reflects a convex-upwards surface slope in that cell. A negative value refers to a concave-upward surface slope. A value of 0 refers to a flat surface (Mancini *et al*., 2010, Xu *et al.*, 2012). These parameters were derived using a 3 x 3 moving window in ArcGIS (Esri, 2012). The slope curvature ranges between 26.41 to –24.86 (Fig.9B). **5)** HI is an appropriate index to identify the evolutionary stage of landscape development (Othman and Gloaguen, 2013b, Pérez-Peña *et al*., 2009 and Strahler, 1952). HI closely relates to the degree of dissection by the drainage network. Thus, this index provides a way for discriminating between different types of landscapes. HI values above 0.6 indicate elevated landscapes with an entrenched drainage network. HI values between 0.35 and 0.6 correspond to significantly eroded areas with a developed system of V-shaped valleys, and values below 0.35 indicate relatively flat landscapes with a low degree of incision (Pérez-Peña *et al*., 2009). The HI map was computed using 100 pixels (~1.5 Km) moving window. The HI ranges between 0.06 and 0.79 (Fig.10A). According to (Pike and Wilson, 1971) the HI of a given area can be estimated using the following equation:

$$HI = \frac{Elevation_{mean} - Elevation_{minimum}}{Elevation_{mmaximum} - Elevation_{minimum}} \quad \ldots\ldots\ldots\ldots\ldots\ldots \; 2$$

(6) Furthermore, TPI are used (equations 3 and 4) as a predictive factor. It represents the variation between the elevation of a pixel (E_C) and the average elevation (E_A) around this pixel. The numbers of pixels defining the area around (n_M) are set by the kernel-matrix (M). The TPI is calculated using equations 3 and 4; (De Reu *et al*., 2013 and Weiss, 2001):

$$TPI = E_C - E_A \quad \ldots\ldots\ldots\ldots\ldots\ldots \; 3$$

$$E_A = \frac{1}{n_M} \sum_{i \in M} E_i \quad \ldots\ldots\ldots\ldots\ldots\ldots \; 4$$

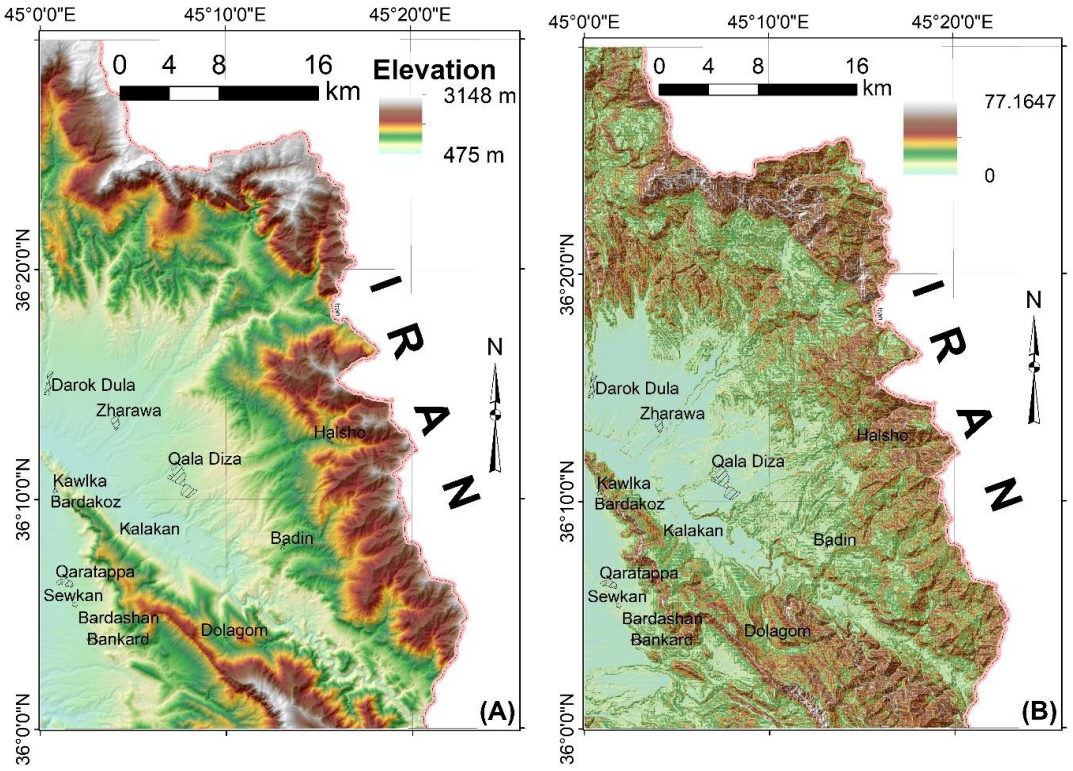

Fig.8: Maps of the landslide geological prediction factors:
A) Elevation; **B)** Slope gradient

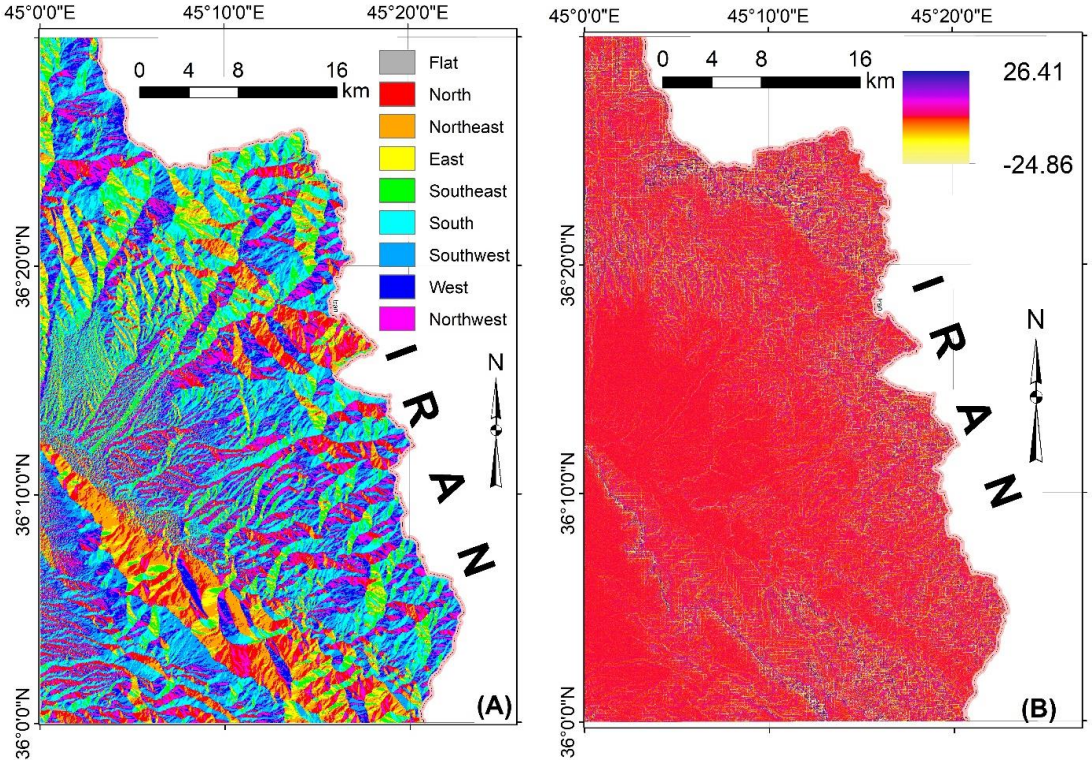

Fig.9: Maps of the landslide geological prediction factors:
A) Slope aspect; **B)** Slope curvature

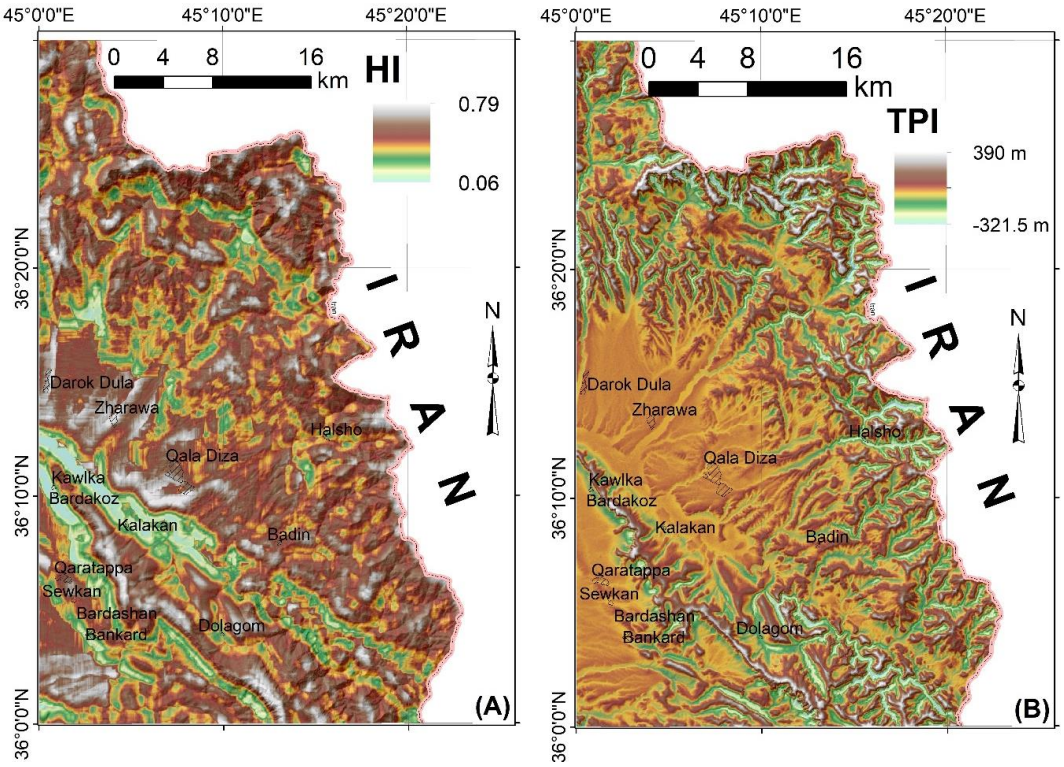

Fig.10: Maps of the landslide geological prediction factors: **A)** HI; **B)** TPI

TPI is the Topographic Position Index, negative TPI values indicate that the central pixel is situated lower than its average surroundings; while positive TPI values indicate that the central pixel is located higher. We have implemented a script in the TecDEM toolbox in order to compute the TPI for the studied area. We used a moving window of 100 pixels (~1.5 Km). Though HI and TPI have been widely used by geomorphologists to classify landscapes, few landslide susceptibility studies explored these indices as predictive factors (Lin *et al.*, 2011). The TPI ranges from 390 to – 321.5 m (Fig.10B).

The factors which describe the drainage pattern are included in the model of landslide susceptibility. We calculate **(7)** the distance to drainage for each point in the study area by making a buffer distance surrounding the drainage network. The farthest point in the map area from the drainage is 2130.6 m (Fig.11A). Finally, calculation of the buffers surrounding roads are used to calculate the **(8)** distance of each point in the study area to roads. The farthest point in the map area from the road is 16778.1 m in the north east of the study area (Fig.11B).

- **Geological Factors**

Lithological and structural variations affect the strength and stability of materials (Ayalew and Yamagishi, 2005). Thus, two geological factors are used as input parameters: **1)** lithology (Fig.3), and **2)** distance to faults. The lithological and the faults factors at the Qala Diza area are explained previously. Calculations of the buffers surrounding the faults are used to calculate the distance to faults. The farthest point in the study area from a fault is 12843.5 m in the west of the study area (Fig.12A).

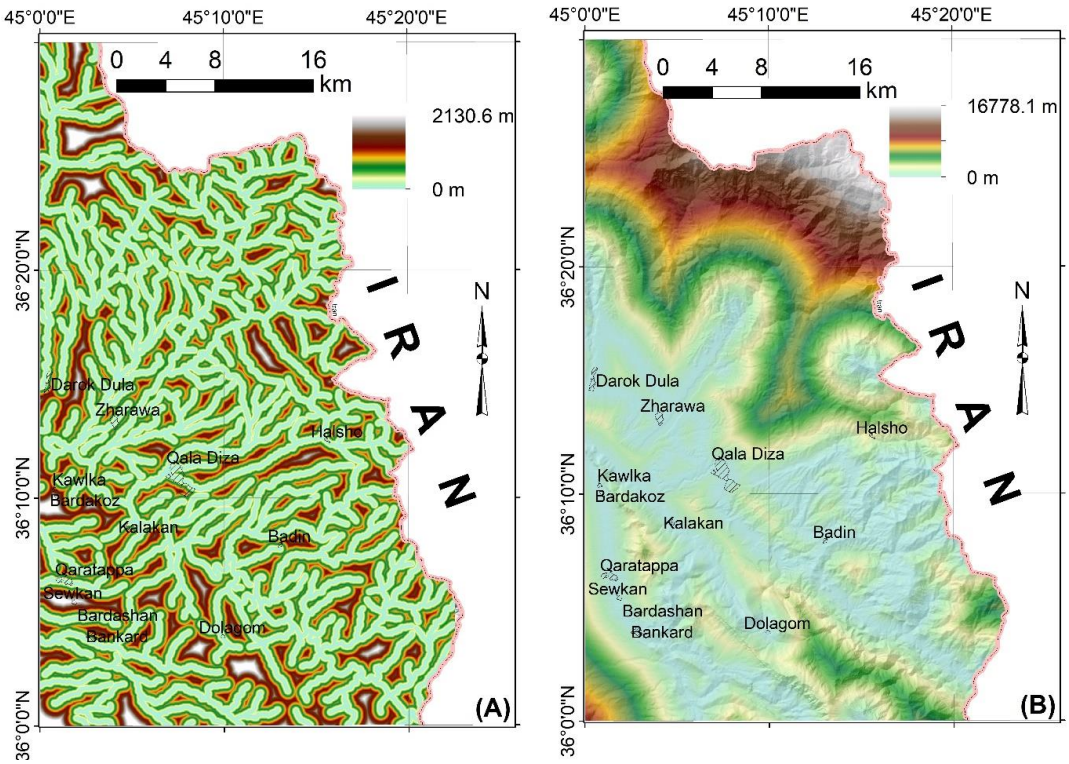

Fig.11: Maps of the landslide geological prediction factors:
A) Distance to drainage, **B)** Distance to road

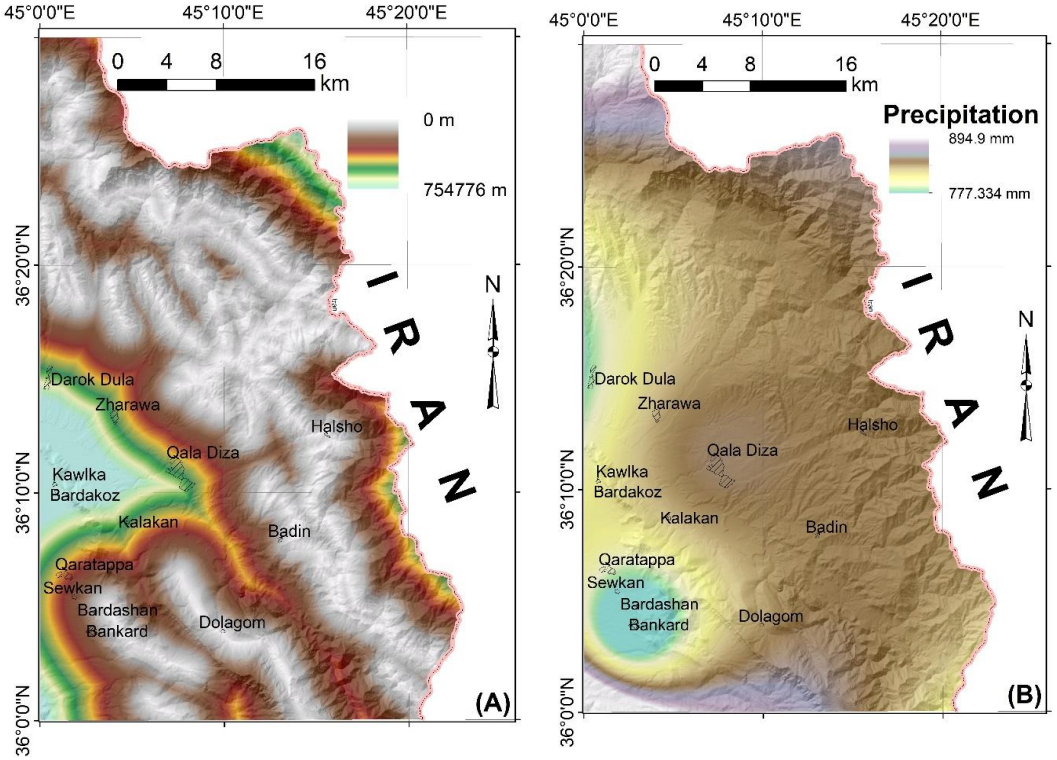

Fig.12: Maps of the landslide geological prediction factors:
A) Distance to fault **B)** Precipitation

- **Environmental Factors**

Two environmental predictive factors are used: land cover, and precipitations. **First)** The land cover map (Al-Saady *et al.*, 2011) was provided by GEOSURV– Iraq and contains thirteen classes. It was created using Landsat satellite data (acquired in 2010) with overall accuracy of ~93.14 (Al-Saady *et al.*, 2011). Thirteen classes of land use and land cover are derived in the study area. These are **(1)** Urban and built-up lands, **(2)** Vegetated land, **(3)** Cultivated land, **(4)** Irrigation land, **(5)** Burn land, **(6)** Harvested land, **(7)** Igneous and/or Metamorphic rocks, **(8)** Conglomerate, **(9)** Carbonate rocks, **(10)** Mixed barren land rocks, **(11)** lake, **(12)** river and channel and **(13)** wetlands (Fig.13). **Second)** Precipitation data from seven climatological stations located within and surrounding of the study area (Qala Diza, Binkard, Choman, Gridjan, Rania, Dukan, and Mawat) is used. The available data covers a period of 7 years (2000 – 2006). However, the limited amount of stations in the study area does not allow to capture local scale variations in precipitations, but it is noticed that the precipitation increases from south towards north of (Fig.12B). The average annual precipitation, using the daily time series data, is calculated. In order to obtain a continuous coverage, interpolated point-wise precipitation data using an inverse distance weighting (IDW) method is used. Although the study area is characterized by high annual precipitation (~777 – 894 mm), but there are small variations in the annual rainfall (<117 mm). The effect of the precipitation in the model is not significant compared to the other factors because of the small amount of precipitation in the study area.

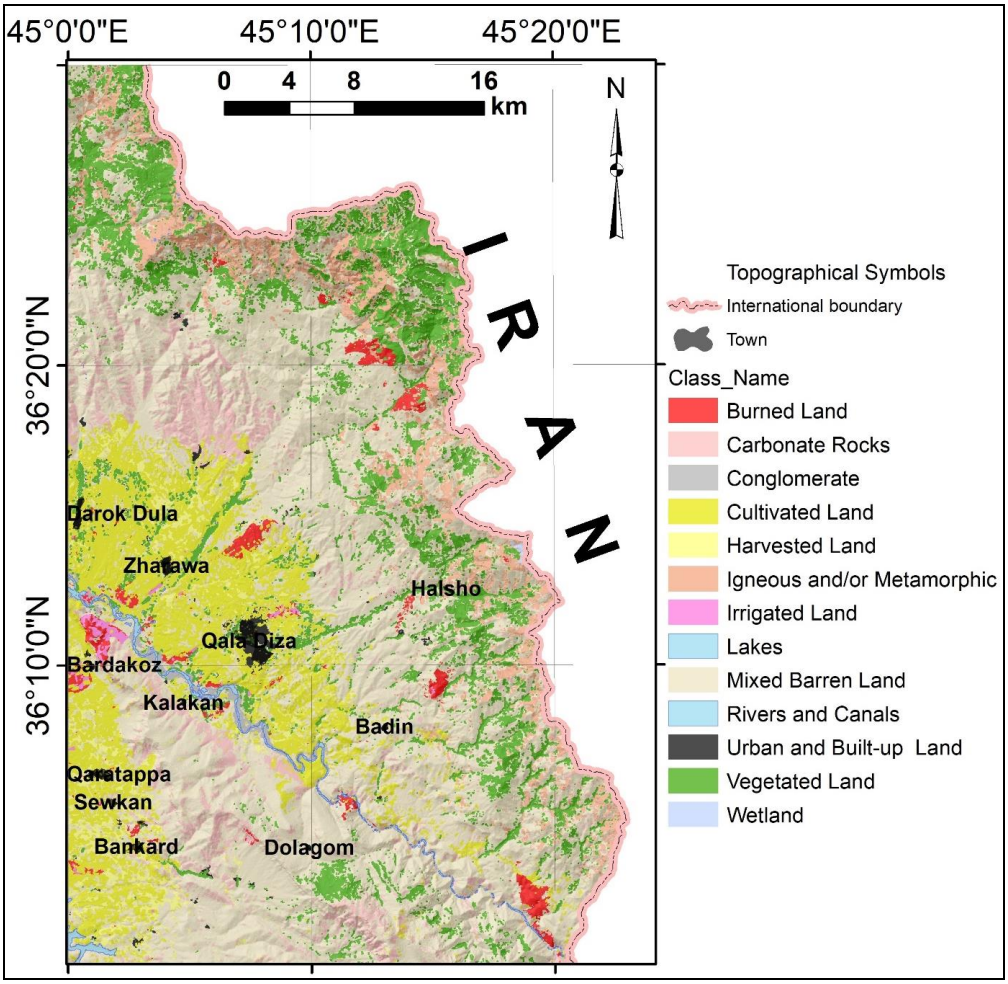

Fig.13: Maps of the Land Use-Land Cover map prediction factor

- **Landslide Susceptibility Models**

The resulting accuracy of the landslide susceptibility depends on the model used (Chen *et al.*, 2012). In this study, the spatial relationship between landslide locations and each predicting factor for land sliding was derived using the logistic regression model. It is a multivariate statistical regression analysis. The model has been widely applied for landslide susceptibility mapping (Guzzetti *et al.*, 1999). The results range between one and zero, where one corresponds to the presence and zero to the absence of landslides, respectively (Althuwaynee *et al.*, 2014). The logistic regression model is expressed as equations (5 and 6) (Kleinbaum and Klein, 2011):

$$P = \frac{1}{1 + e^{-z}} \quad \ldots\ldots\ldots\ldots\ldots\ldots\ldots\ldots\ldots \quad 5$$

$$z = a + \beta 1\ X1 + \beta 2\ X2 + \ldots + \beta nXn \quad \ldots\ldots\ldots\ldots\ldots\ldots \quad 6$$

where a is the intercept of the model, n is the number of variables, β are the β values associated with each of the independent variables, P is the probability, which varies between 0 and 1 on an S-shaped curve and z varies from $-\infty$ to $+\infty$ on an S-shaped curve.

- **Preparation of Training Dataset**

The inventory map is used, by classifying the boundaries of each landslide polygon into two zones: **1)** the landslide depletion zone and **2)** the landslide accumulation zone. The geometrical attributes are stored in a GIS database as a shape file and then we have rasterized the polygons by 30 m resolution. Only the depletion zones of the landslides are included in the susceptibility analysis (Van Den Eeckhaut *et al.*, 2006).

The total number of the landslide pixels is 38996. The logistic regression model need a training dataset containing both pixels with landslides and pixels without landslides (Ayalew *et al.*, 2005 and Ozdemir and Altural, 2013). Therefore, we randomly selected 38961 pixels from the stable slopes (without landslides) and used them, in addition to the landslide pixels to derive the coefficient of the logistic regression model. Following literature suggestions (Xu *et al.*, 2012), we sub-divided the input pixels (77957 pixels) randomly into training and validation data subsets. The training dataset included 80% of the input pixels and the validation set included the remaining 20% of the input pixels.

The predicted factors represent the independent variables, while the class values (landslide-present and landslide-absent), i.e. 0 and 1 are the dependent variables. The pixels with information from the predictive factors were exported and saved as a text file. This file was analyzed using R software to obtain the estimation constants (α and β), which are important for calculating the probability (z).

- **Predicting factors in Qala Diza area**

About 2.59 % of the study area suffer from landslides. The landslide susceptibility maps have been prepared using logistic regression model. The training pixels were used to derive the coefficients of logistic regression. The model-building process for logistic regression started with 12 prediction factors. The landslide prediction factors considered in this study are shown in Table (2). In the last processing step, nine factors were interpreted as non-significant (p-value > 0.05) and therefore were excluded from the analysis. We used the significant nine remaining factors (p-value < 0.05), namely: lithology, slope gradient, HI, elevation, distance to drainage, distance to faults, distance to roads, precipitation, and TPI (Table 2).

Table 2: Results obtained for the logistic regression model

No.	Coefficient	Odd ratio of logistic
1	HI	1532.39
2	Lithology	36
3	Slope gradient	1.04
4	Topographic position index (TPI)	1
5	Distance to roads	1
6	Distance to faults	1
7	Distance to drainage	1
8	Elevation	1
9	Precipitation	0.95

The obtained odd ratios are shown in Table (2). The factors with an odd ratio of more than 1 (HI, lithology, slope gradient) are positively related to the landslide susceptibility, while the precipitation factor with less than 1 is negatively related. Factors with an odd ratio of 1, like elevation and distance to drainage, are neutral in detecting the landslide susceptibility, in the study area. The susceptibility map was zoned into five zones (Fig.14).

The HI is the morphometric feature, which significantly increases the prediction accuracy of the landslide susceptibility and using it, as a predictive factor, increases the areas under the curve of the landslide susceptibility maps. The HI is a good indicator for erosional processes related to the mass wasting and illustrates the stage of vertical and lateral erosion. The index value decreases when the amount of landmass volume, removed by erosion, increases (Strahler, 1952). Thus, HI allows to summarize how landscapes respond to erosion.

Different lithological units have different susceptibility to landslides (Ozdemir and Altural, 2013). As a result, the wide variation of the exposed lithological types in the Qala Diza area makes the lithology a major prediction factor (Table 2). The more stable units are the Naokelekan, Barsarin and Chia Gara formations. The slope in these formations is mostly low. They are composed of tough limestone and dolomitic limestone, which reduce the landslides occurrences. The rocks of the Walash Group have more unstable slopes due to weakness zones between rocks that can be easily weathered. The fieldwork observations showed that the weathered rocks of the Walash Group showed a behavior similar to soil materials. The presence of soils rich in clay makes the slopes unstable. The limestone beds include many slides. These rocks are affected by numerous joints and fractures, which may facilitate water infiltration as well as weathering. Although the Qala Diza area is characterized by a rough topography, but the slope gradient has a lower range of estimation weight than the HI and the lithology.

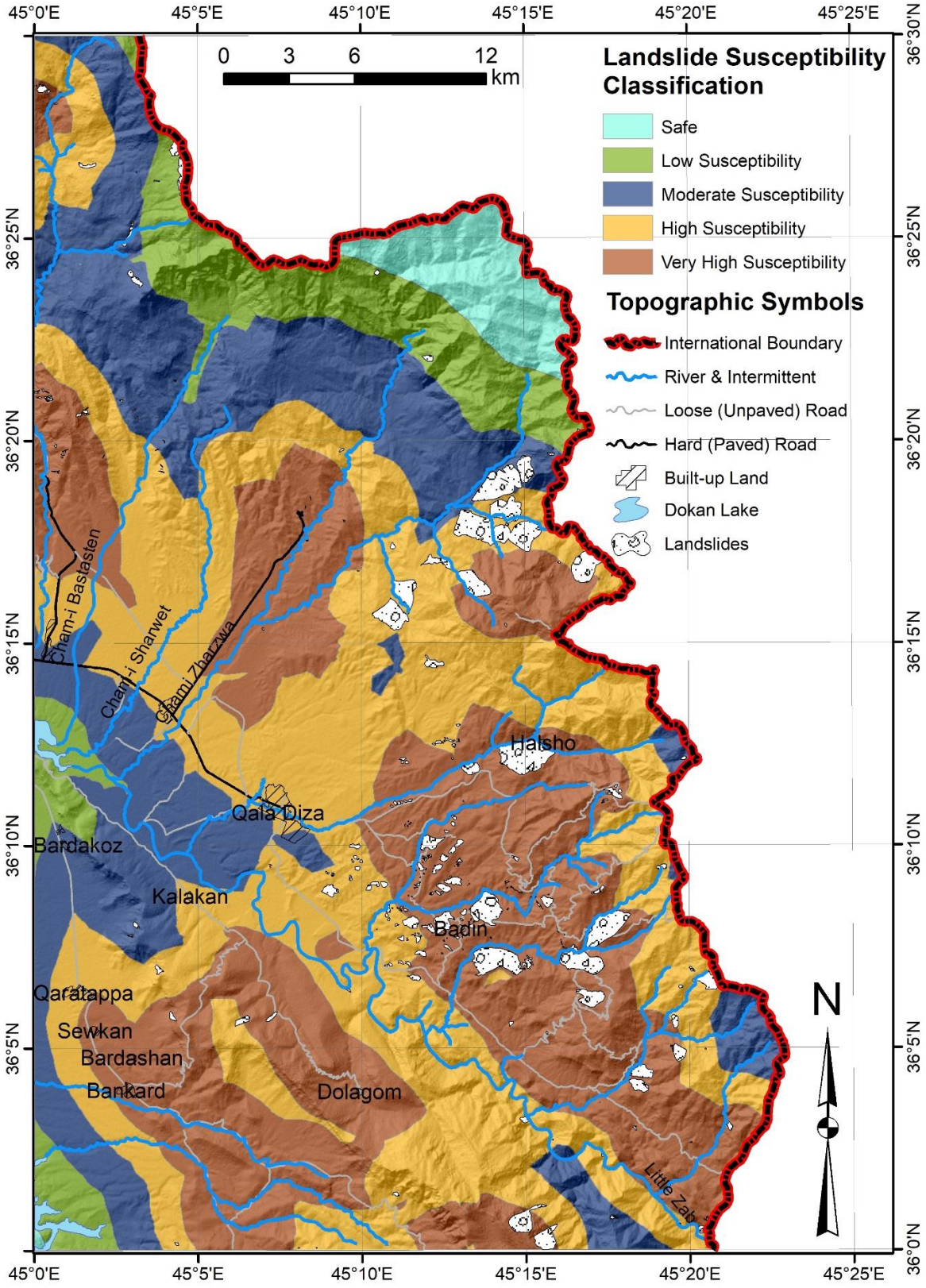

Fig.14: Landslide Susceptibility Map of Qala Diza area with the present landslide

- **Landslide Susceptibility in Qala Diza Area**

In order to recognize the best susceptibility model, we applied quantitative measurement called the areas under the curve of the prediction rate curve as a prediction skill method to the landslide validation datasets (20% of the total landslide pixels). The areas under the curve is widely used to estimate the accuracy of landslide susceptibility models (Yesilnacar and Topal, 2005). A prediction rate curve is a two-dimensional plot. The x-axis is (100 – landslide susceptibility rank %) and the y-axis is the cumulative percentage of validation landslide occurrence (%). An acceptable model should have an area under the curve of more than 50% (Chung *et al*., 2014).

The landslide susceptibility values given by the logistic regression model was then classified using natural breaks technique into five susceptibility classes: Very High, High, Moderate, Low and Safe (Mărgărint *et al.*, 2013, Ozdemir and Altural, 2013 and Shahabi *et al.*, 2014). We have used natural breaks method because it allows to gather similar values and to maximize the differences between classes. Natural breaks are useful when the landslide susceptibility histogram shows distinct breaks (Mărgărint *et al.*, 2013). The logistic regression model (Fig.15) shows that the area under the curve is 85.15%. About 82% of the landslides are located in the High and Very High landslide susceptibility prediction zone, whereas, only ~3% of the landslides fall in the other zones (Moderate, Low and Safe), which means that our model is authentic and can be trusted in the landslide prediction processes.

The study area includes 368 villages, among them, 180 villages, such as Bingrd, Qadir Agh, Sardarwan and Zawita are located in the Very High landslide susceptibility zone. These villages are under the threat of landslides risk. The Very High and High susceptibility areas are located in the east and center of the study area. Bardqalsht and Gazohrahzi Mountains are among the High susceptibility areas.

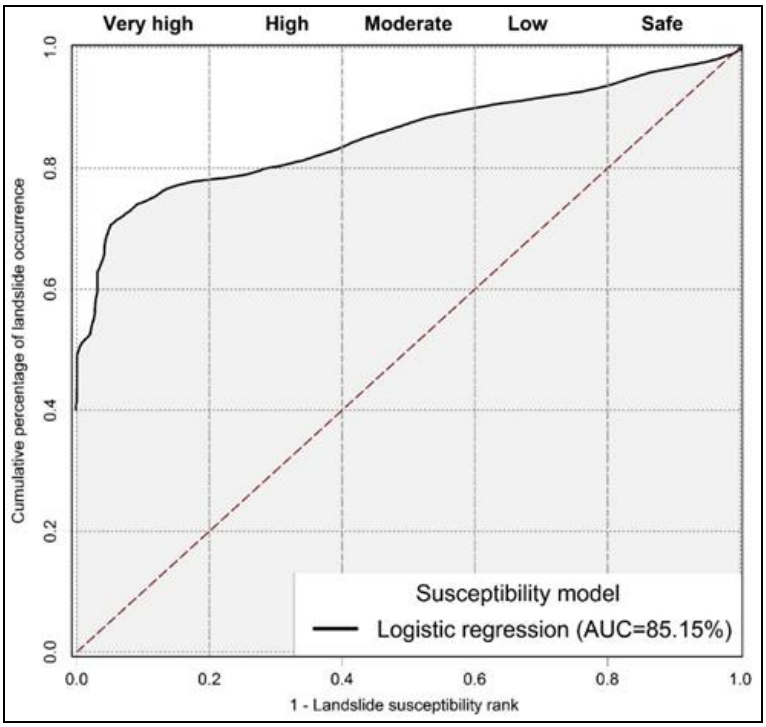

Fig.15: Prediction rate curve plot evaluation of the logistic regression method

CONCLUSIONS

The reference inventory derived in this study is based on 353 landslides (representing a cumulated surface of ~35 Km^2), which were mapped from twelve Quick Bird scenes using manual delineation. Rock falls, transitional slides and slumps landslides have occurred in different lithological units. We have first analyzed cumulative landslide number-size distributions using the inventory map. The maximum distribution of landslides within the study area ranges from 0.001 to 0.1 Km^2. The largest 12 landslides (>1 Km^2) cover a total area of 18.8 Km^2, located in the northeast– east of the study area. The cumulative distributions of the landslides show statistical correlations of >0.894. The power exponent was $\alpha = -0.425$.

Twelve prediction factors are utilized in this study, most of which were derived from Digital Elevation Model (DEM) of Shuttle Radar Topography Mission (SRTM), in addition to geological and environmental factors. Two of the prediction factors (HI and lithology) have more influence than other factors in landslide occurrences. Morphometric factors proved to be useful in our study area. The use of morphometric indices as prediction factor significantly increases the estimation accuracy of the landslide susceptibility. The significant increase in accuracy estimation is related to the susceptibility of these indices to erosional processes. The HI allows to discriminate between different types of ridges and valleys and slightly improve the models accuracies. It shows that the HI yields better results than slope curvatures, and increases the area under the curve.

The results obtained in this study indicate that the logistic regression model is a reliable estimator for the landslide susceptibility. The areas under the curve of the prediction rate curve for the landslide susceptibility shows that the accuracy of the map is 85.15%. One hundred eighty villages in the Qala Diza map are located in the Very High landslide susceptible areas and are under serious threat of landslide hazards.

REFERENCES

Abdulaziz, M.T., Ibraheem, F.A., Sebesta, J. and Hassan, A., 1983. The Lesser Zab River Basin project, photo-engineering geological and geomorphological mapping. GEOSURV, Baghdad, Iraq.

Akgun, A., 2012. A comparison of landslide susceptibility maps produced by logistic regression, multi-criteria decision, and likelihood ratio methods: a case study at İzmir, Turkey. Landslides. Vol.9, No.1, p. 93 –106.

Alavi, M., 1994. Tectonics of Zagros Oroginic Belt of Iran: new data and interpretations. Tectonophysics. Vol.229, No. 3 – 4, p. 221 – 238.

Alavi, M., 2004. Regional stratigraphy of the Zagros Fold – Thrust Belt of Iran and its proforeland evolution. Am J Sci. Vol. 304, No.1, p. 1 – 20.

Al-Saady, Y.I., Al-Ma′amar, A.F., Al-Saati, R.M. and Al-Dulaimi, T.Y., 2011. Series of land use land cover maps of Iraq scale 1:250 000, Erbil and Mahabad quadrangle sheet NI-38-14 and NI-38-15 (LULCM 5 and 6). Baghdad, Iraq, GEOSURV, int. rep. no. 3360.

Althuwaynee, O.F., Pradhan, B., Park, H.–J. and Lee, J.H., 2014. A novel ensemble bivariate statistical evidential belief function with knowledge-based analytical hierarchy process and multivariate statistical logistic regression for landslide susceptibility mapping. Catena. Vol.114, p. 21 – 36.

Atkinson, P.M. and Massari, R., 1998. Generalised linear modelling of susceptibility to landsliding in the central Apennines, Italy. Comput Geosci. Vol.24, No.4, p. 373 – 385.

Ayalew, L .and Yamagishi, H., 2005. The application of GIS–based logistic regression for landslide susceptibility mapping in the Kakuda – Yahiko Mountains, Central Japan. Geomorphology. Vol.65, No. 1 – 2, p. 15 – 31.

Ayalew, L., Yamagishi, H., Marui, H. and Kanno, T., 2005. Landslides in Sado Island of Japan: Part II. GIS – based susceptibility mapping with comparisons of results from two methods and verifications. Eng Geol. Vol.81, No.4, p. 432 – 445.

Blasio, F.V.D., 2011. Introduction to the physics of landslides: lecture notes on the dynamics of mass wasting. Springer, New York, 405pp.

Bolton, C.M., 1954. Geological map kurdistan series, scale 1:100 000, sheet k4, Rania. Baghdad, Iraq, GEOSURV, int. rep. no. 271.

Brink, U.S.t., Barkan, R., Andrews, B.D. and Chaytor, J.D., 2009. Size distributions and failure initiation of submarine and subaerial landslides. Earth Planet Sci Lett. Vol.287, No.1 – 2, p. 31 – 42.

Buday, T. and Suk, M., 1978. Report on the geological survay in NE Iraq between Halabja and Qala'a Diza. Baghdad, Iraq, GEOSURV, int. rep. no.950.

Capitani, M., Ribolini, A. and Bini, M., 2013. The slope aspect: A predisposing factor for landsliding? Comptes Rendus – Geoscience. Vol.345, No. 11 – 12, p. 427 – 438.

Carrara, A., Cardinali, M., Guzzetti, F. and Reichenbach, P., 1995. GIS Technology in Mapping Landslide Hazard. In: A. Carrara and F. Guzzetti (Editors), Geographical Information Systems in Assessing Natural Hazards. Advances in Natural and Technological Hazards Research. Springer Netherlands, p. 135 – 175.

Chen, W., Li, X., Wang, Y. and Liu, S., 2012. Landslide susceptibility mapping using LiDAR and DMC data: a case study in the Three Gorges area, China. Environmental Earth Sciences. Vol.70, No.2, p. 673 – 685.

Choi, J., Oh, H.–J., Lee, H.–J., Lee, C. and Lee, S., 2012. Combining landslide susceptibility maps obtained from frequency ratio, logistic regression, and artificial neural network models using ASTER images and GIS. Eng Geol. Vol.124, No.1, p. 12 – 23.

Chung, J.–w., Rogers, J.D. and Watkins, C.M., 2014. Estimating severity of seismically induced landslides and lateral spreads using threshold water levels. Geomorphology. Vol.204, p. 31 – 41.

Conforti, M., Pascale, S., Robustelli, G. and Sdao, F., 2014. Evaluation of prediction capability of the artificial neural networks for mapping landslide susceptibility in the Turbolo River catchment (northern Calabria, Italy). Catena. Vol.113, , p. 236 – 250.

Corominas, J. and Moya, J., 2010. Contribution of dendrochronology to the determination of magnitude – frequency relationships for landslides. Geomorphology. Vol.124, No. 3 – 4, p. 137 – 149.

Dai, F.C., Xua, C., Yao, X., Xua, L., Tu, X.B. and Gong, Q.M., 2011. Spatial distribution of landslides triggered by the 2008 Ms 8.0 Wenchuan earthquake, China. J Asian Earth Sci. Vol.40, No.4, p. 883 – 895.

De Reu, J., Bourgeois, J., Bats, M., Zwertvaegher, A., Gelorini, V., De Smedt, P., Chu, W., Antrop, M., De Maeyer, P., Finke, P., Van Meirvenne, M., Verniers, J. and Crombé, P., 2013. Application of the topographic position index to heterogeneous landscapes .Geomorphology. Vol.186, p. 39 – 49.

Dikau, R., Brunsden, D., Schrott, L. and Ibsen, M.L., 1996. Landslide Recognition: Identification,Movement and Causes, 274pp.

Ercanoglu, M., 2005. Landslide susceptibility assessment of SE Bartin (West Black Sea region, Turkey) by artificial neural networks. Nat Hazards Earth Syst Sci. Vol.5, No.6, p. 979 – 992.

ESRI, E.S.R.I., 2011. ArcGIS Desktop: Release 10. Environmental Systems Research Institute, Redlands, CA., 2012. ArcGIS help library

Fouad, S.F., 2012. Tectonic map of Iraq, scale 1:1000 000 In: Third (Editor). GEOSURV, Baghdad, Iraq.

Fujii, Y., 1969. Frequency distribution of landslides caused by heavy rainfall. Journal Seismological Society of Japan. Vol.2, p. 244 – 247.

Fukuoka, H., Sassa, K., Wang, G., Wang, F., Wang, Y. and Tian, Y., 2005. Landslide risk assessment and disaster management in the imperial resort palace of Lishan, Xian, China (C101–4). In: K. Sassa, H. Fukuoka, F. Wang and G. Wang (Editors), United Nation world conference on disaster reduction (WCDR). Springer, Kobe, Japan, p. 81 – 89.

García-Rodríguez, M.J. and Malpica, J.A., 2010. Assessment of earthquake-triggered landslide susceptibility in El Salvador based on an artificial neural network model. Natural Hazards and Earth System Science. Vol.10, No.6, p. 1307 – 1315.

García-Rodríguez, M.J., Malpica, J.A., Benito, B .and Díaz, M., 2008. Susceptibility assessment of earthquake-triggered landslides in El Salvador using logistic regression. Geomorphology. Vol.95, No. 3 – 4, p. 172 – 191.

GEOSURV, 1985. Geological Quaderangle Map of Qala Diza Scale of 1:100,000.

Guthrie, R.H. and Evans, S.G., 2004. Magnitude and frequency of landslides triggered by a storm event, Loughborough Inlet, British Columbia. Nat Hazards Earth Syst Sci. Vol.4, p. 475 – 483.

Guzzetti, F., Cardinali, M., Reichenbach, P. and Carrara, A., 2000. Comparing Landslide Maps: A Case Study in the Upper Tiber River Basin, Central Italy. Environmental Management. Vol.25, No.3, p. 247 – 263.

Guzzetti, F., Carrara, A., Cardinali, M. and Reichenbach, P., 1999. Landslide hazard evaluation: a review of current techniques and their application in a multi-scale study, Central Italy. Geomorphology. Vol.31, No. 1 – 4, p. 181 – 216.

Guzzetti, F., Malamud, B.D., Turcotte, D.L. and Reichenbach, P., 2002. Power-law correlations of landslide areas in central Italy. Earth and Planetary Science Letters. Vol.195, No. 3 – 4, p. 169 – 183.

Guzzetti, F., Reichenbach, P., Cardinali, M., Galli, M. and Ardizzone, F., 2005. Probabilistic landslide hazard assessment at the basin scale. Geomorphology. Vol.72, No. 1 – 4, p. 272 – 299.

Jassim, S.Z. and Goff, J.C., 2006. Geology of Iraq. Dolin, Prague and Moravian Museum, Brno. 341pp.

Kayastha, P., Dhital, M.R. and De Smedt, F., 2013. Application of the analytical hierarchy process (AHP) for landslide susceptibility mapping: A case study from the Tinau watershed, west Nepal. Comput Geosci. Vol.52, p. 398 – 408.

Kleinbaum, D.G. and Klein, M., 2011. Survival Analysis: A Self-Learning Text, Third Edition. Springer.

Kottek, M., Grieser, J., Beck, C., Rudolf, B. and Rubel, F., 2006. World Map of the Köppen – Geiger climate classification. Meteorol Z. Vol.15, No.3, p. 259 – 263.

Lee, S., 2013. Landslide detection and susceptibility mapping in the Sagimakri area, Korea using KOMPSAT–1 and weight of evidence technique. Environmental Earth Sciences. Vol.70, No.7, p. 3197 – 3215.

Lee, S., Choi, J., Chwae, U. and Chang, B., 2002. Landslide susceptibility analysis using weight of evidence, p. 2865 – 2867.

Lee, S. and Min, K., 2001. Statistical analysis of landslide susceptibility at Yongin, Korea. Environ Geol. Vol.40, No.9, p. 1095 – 1113.

Lee, S., Ryu, J., Min, K. and Won, J., 2001. Development of two artificial neural network methods for landslide susceptibility analysis, p. 2364 – 2366.

Lee, S. and Talib, J.A., 2005. Probabilistic landslide susceptibility and factor effect analysis. Environ Geol. Vol.47, No.7, p. 982 – 990.

Lin, L.L., Wang, C.W., Chiu ،C.L. and Ko, Y.C., 2011. A study of rationality of slopeland use in view of land preservation. Paddy and Water Environment. Vol.9, No.2, p. 257 – 266.

Mancini, F., Ceppi, C. and Ritrovato, G., 2010. GIS and statistical analysis for landslide susceptibility mapping in the Daunia area, Italy. Natural Hazards and Earth System Science. Vol.10, No.9, p. 1851 – 1864.

Mantovani, F., Soeters, R. and Van Westen, C.J., 1996. Remote sensing techniques for landslide studies and hazard zonation in Europe. Geomorphology. Vol.15, No. 3 – 4 SPEC. ISS., p. 213 – 225.

Mărgărint, M.C., Grozavu, A. and Patriche, C.V., 2013. Assessing the spatial variability of coefficients of landslide predictors in different regions of Romania using logistic regression. Nat Hazards Earth Syst Sci . Vol.13, No.12, p. 3339 – 3355.

McQuarrie, N., Stock, J.M., Verdel, C. and Wernicke, B.P., 2003. Cenozoic evolution of Neotethys and implications for the causes of plate motions. Geophys Res Lett. Vol.30, No.20, p. 2 – 6.

Metternicht, G., Hurni, L. and Gogu, R., 2005. Remote sensing of landslides: An analysis of the potential contribution to geo-spatial systems for hazard assessment in mountainous environments. Remote Sens Environ. Vol.98, No. 2 – 3, p. 284 – 303.

Michoud, C., Jaboyedoff, M., Derron, M.H., Nadim, F. and Leroi, E., 2012. New classification of landslide-inducing anthropogenic activities. EGU General Assembly Conference Abstracts. Vol.14, 2923pp.

Moghadam, H.S., Stern, R.J., Chiaradia, M. and Rahgoshay, M., 2013. Geochemistry and tectonic evolution of the Late Cretaceous Gogher-Baft ophiolite, central Iran. Lithos. Vol.168 – 169, p. 33 – 47.

Nefeslioglu, H.A., Duman, T.Y. and Durmaz, S., 2008a. Landslide susceptibility mapping for a part of tectonic Kelkit Valley (Eastern Black Sea region of Turkey). Geomorphology. Vol.94, No. 3 – 4, p. 401 – 418.

Nefeslioglu, H.A., Gokceoglu, C. and Sonmez, H., 2008b. An assessment on the use of logistic regression and artificial neural networks with different sampling strategies for the preparation of landslide susceptibility maps. Eng Geol. Vol.97, No. 3 – 4, p. 171 – 191.

Othman, A. and Gloaguen, R., 2013a. Automatic extraction and size distribution of landslides in Kurdistan Region, NE Iraq. Remote Sensing. Vol.5, No.5, p. 2389 – 2410.

Othman, A. and Gloaguen, R., 2013b. River courses affected by landslides and implications for hazard assessment: a high resolution remote sensing case study in NE Iraq – W Iran. Remote Sensing. Vol.5, No.3, p. 1024 – 1044.

Othman, A. and Gloaguen, R., 2015. Landslide susceptibility mapping in Mawat area, Kurdistan Region, NE Iraq: a comparison of different statistical models. NHESSD. Vol 3., No.3, p. 1789 – 1833.

Ozdemir, A. and Altural, T., 2013. A comparative study of frequency ratio, weights of evidence and logistic regression methods for landslide susceptibility mapping: Sultan Mountains, SW Turkey. J Asian Earth Sci. Vol.64, p. 180 – 197.

Paver, G.L. and Scholtzh, H.C., 1955. Six Monthly report July to December 1955 (volume 5). Baghdad, Iraq, GEOSURV, int. rep. no. 266.

Pelletier, J.D., Malamud, B.D., Blodgett, T. and Turcotte, D.L., 1997. Scale-invariance of soil moisture variability and its implications for the frequency-size distribution of landslides. Eng Geol. Vol.48, No.3 – 4, p. 255 – 268.

Peng, L., Niu, R., Huang ،B., Wu, X., Zhao, Y. and Ye, R., 2014. Landslide susceptibility mapping based on rough set theory and support vector machines: A case of the Three Gorges area, China. Geomorphology. Vol.204, p. 287 – 301.

Pérez-Peña, J.V., Azañón, J.M. and Azor, A., 2009. CalHypso: An ArcGIS extension to calculate hypsometric curves and their statistical moments. Applications to drainage basin analysis in SE Spain. Comput Geosci. Vol.35, No.6, p. 1214 – 1223.

Petley, D., 2012. Global patterns of loss of life from landslides. Geology. Vol.40, No.10, p. 927 – 930.

Pike, R.J. and Wilson, S.E., 1971. Elevation-relief ratio, hypsometric integral, and geomorphic area–altitude analysis. Bull Geol Soc Am. Vol.82, No.4, p. 1079 – 1084.

Qiao, G., Lu, P., Scaioni, M., Xu, S., Tong, X., Feng, T., Wu, H., Chen, W., Tian, Y., Wang, W. and Li, R., 2013. Landslide investigation with remote sensing and sensor network: From susceptibility mapping and scaled-down simulation towards in situ sensor network design. Remote Sensing. Vol.5, No.9, p. 4319 – 4346.

Shahabi, H., Khezri, S., Ahmad, B.B. and Hashim, M., 2014. Landslide susceptibility mapping at central Zab basin, Iran: A comparison between analytical hierarchy process, frequency ratio and logistic regression models. Catena. Vol.115, p. 55 – 70.

Sissakian, V.K., 1998. The Geology of Erbil and Mahabad Quadrangle Sheet NJ-38-14 and NJ-38-15 (GM 5 and 6) Scale 1: 250 000.

Sissakian, V.K. and Fouad, S.F., 2014. The Geology of Erbil and Mahabad Quadrangles, scale 1: 250 000, sheets No .NJ-38-14 and NJ-38-15, Baghdad, Iraq.

Strahler, A.N., 1952. Hypsometric (area-altitude) analysis of erosional topography. Geol Soc Am Bull. Vol.63, No.11, p. 1117 – 1142.

Sugai, T., Ohmori, H. and Hirano, M., 1995. Rock control on magnitude-frequency distribution of landslide. Transactions Japan Geomorphology Union Vol.15, No.3, p. 233 – 251.

USGS, 2004. https://pubs.usgs.gov/fs/2004/3072/

Van-Den-Eeckhaut, M., Poesena, J., Goversa, G., Verstraeten, G. and Demoulinc, A., 2007. Characteristics of the size distribution of recent and historical landslides in a populated hilly region. Earth Planet Sci Lett. Vol.256, No. 3 – 4, p. 588 – 603.

Van Den Eeckhaut, M., Vanwalleghem, T., Poesen, J., Govers, G., Verstraeten, G. and Vandekerckhove, L., 2006. Prediction of landslide susceptibility using rare events logistic regression: A case-study in the Flemish Ardennes (Belgium). Geomorphology. Vol.76, No. 3 – 4, p. 392 – 410.

Varnes, D.J., 1978. Slope movement types and processes., Washington D.C., Landslides: analysis and contro:. Chapter 2, p. 11 – 33.

Wang, L.J., Sawada, K. and Moriguchi, S., 2013. Landslide susceptibility analysis with logistic regression model based on FCM sampling strategy. Comput Geosci. Vol.57, p. 81 – 92.

Weiss, A.D., 2001. Topographic position and landforms analysis, ESRI users conference, San Diego, CA.

Werner, E.D. and Friedman, H.P., 2010. Landslides: Causes, types and effects. Nova Science Publishers, New York, 404pp.

Xu, C., Xu, X., Dai, F. and Saraf, A.K., 2012. Comparison of different models for susceptibility mapping of earthquake triggered landslides related with the 2008 Wenchuan earthquake in China. Comput Geosci. Vol.46, p. 317 – 329.

Yalcin, A., Reis, S., Aydinoglu, A.C. and Yomralioglu, T., 2011. A GIS–based comparative study of frequency ratio, analytical hierarchy process, bivariate statistics and logistics regression methods for landslide susceptibility mapping in Trabzon, NE Turkey. Catena. Vol.85, No.3, p. 274 – 287.

Yao, X., Tham, L.G. and Dai, F.C., 2008. Landslide susceptibility mapping based on Support Vector Machine: A case study on natural slopes of Hong Kong, China. Geomorphology. Vol.101, No.4, p. 572 – 582.

Yesilnacar, E. and Topal, T., 2005. Landslide susceptibility mapping: A comparison of logistic regression and neural networks methods in a medium scale study, Hendek region (Turkey). Eng Geol. Vol.79, No. 3 – 4, p. 251 – 266.

Zêzere, J.L., 1999. Landslide susceptibility assessment considering landslide typology. A case study in the area north of Lisbon (Portugal). Nat Hazards Earth Syst Sci. Vol.2, No. 1/2, p. 73 – 82.

Zhao, C., Lu, Z., Zhang, Q. and de la Fuente, J., 2012. Large-area landslide detection and monitoring with ALOS/PALSAR imagery data over Northern California and Southern Oregon, USA. Remote Sens Environ. Vol.124, p. 348 – 359.

About the authors

Dr. Arsalan Ahmed Othman graduated from Baghdad University in 2000 with B.Sc. degree in Geology, and M.Sc. in Remote Sensing in 2008 from the same university and Ph.D. TU Bergakademie Freiberg/ Germany in 2015. He joined GEOSURV in 2000. He has 9 documented reports in GEOSURV's Library and 11 published papers in deferent journals. He supervised three M.Sc. students in national and international universities. His major field of interest is satellite image interpretation and application for remote sensing and GIS in geology.

e-mail: arsalan.aljaf@gmail.com
Mailing address: Iraq, Sulaimaniyah Qula Raisi

Mr. Azad U. Al-Jaff He obtained the BSc. in petroleum and Mining Engineering – Baghdad University, College of Engineering Since 1991; he has been employed in the Iraqi GEOSURV. He is now is Senior Chief Engineers. Most of his work in the field in the Western Desert of Iraq as supervisor engineer of the drilling operations. Between (1995 to 2003). He worked in the production plant of sodium sulphate, and was developed in the post to be the director of the sodium sulphate factory. He contributed to the development of methods of production and methods of extraction of sodium sulphate from raw clay and from the crystals. He improved the quality of production. Currently, he is in the head of Iraqi GEOSURV in Sulaymaniyah office.

e-mail: azadssy@gmail.com

Dr. Diary A. Al-Manmi, an assistant professor, graduated from University of Baghdad in 1989, with B.Sc. degree in Geology, and he awarded MSc and Ph.D. in 2002 and 2008 from the same University in the field of hydrogeology. Currently; he is a Vice Dean of the College of Science at the University of Sulaimaniyah. He has 16 years of experience working in the field of hydrogeology teaching like hydrology, hydrogeology and groundwater modeling courses and researching. He published eight papers, and supervised eight MSc students inside Iraq and outside of Iraq like Germany, Netherlands, and Hungary. He is member of several national and international societies like International Association of hydrogeologist (IAH) and Kurdistan Geologists-Society. He has a good computer skill and working with much software like MODFLOW, ROCKWORK, SURFER, AQUIFERTEST, PHREEQC, and STATISTICA.

e-mail: diary.amin@univsul.edu.iq

Mr. Ahmed F. Al-Maamar is graduated from University of Baghdad in 1997 with B.Sc. degree in Geology, and M.Sc. degree in remote sensing, Geomorphology and Structural geology from the same university in 2015. He is joined GEOSURV/ Iraq in 2001 and currently working in geology department/ Remote Sensing division. He has 15 documented reports in GEOSURV's Library and 2 published papers in Morphostructure, Remote Sensing and GIS application.

e-mail: ahmedryaman@gmail.com